A molecular dynamics study of water mass accommodation on condensed phase water coated by fatty acid monolayers

S. Takahama[1] and L. M. Russell[1]

Received 28 July 2010; revised 4 October 2010; accepted 13 October 2010; published 21 January 2011.

[1] As the water uptake by particles and clouds influences the radiative balance of the Earth, it is desirable to understand the mechanisms and parameters, which regulate water uptake in these colloidal particles. In this work, molecular dynamics simulations were used to simulate scattering or accommodation of water vapor molecules impinging on a slab of water and slabs of water coated by monomolecular amphiphile films: octanoic acid (C_8) at surface densities of 29 and 18 Å^2 per molecule and myristic acid (C_{14}) at 29 Å^2 per molecule. The mass accommodation coefficient of near unity on a pure water slab is in agreement with values estimated using similar scattering simulations using other potentials for water. The addition of surface-active organic molecules in quantities corresponding to less than 1% of mass in a typical cloud droplet are predicted to reduce this mass accommodation coefficient by 70–100% in similar types of scattering simulations. The mass accommodation coefficient decreased monotonically with projected surface coverage of the hydrocarbon backbones, although the accommodation mechanisms differed by packing density and type of organic molecule. The mechanisms of interaction of the impinging water vapor molecules with the simulated organic films are discussed in the context of their chemical characteristics and physical structures (e.g., fatty acid chain orientation).

Citation: Takahama, S., and L. M. Russell (2011), A molecular dynamics study of water mass accommodation on condensed phase water coated by fatty acid monolayers, *J. Geophys. Res.*, *116*, D02203, doi:10.1029/2010JD014842.

1. Introduction

[2] Prediction of future climate scenarios is limited by our understanding of how atmospheric particles form cloud droplets and how these droplets grow with additional uptake of water vapor [*Intergovernmental Panel on Climate Change* (*IPCC*), 2007], among other factors. The thermodynamics of water uptake is determined by bulk solubility of chemical constituents, particle size, and capacity for surface adsorption and in principle can be investigated through experimental and theoretical models of chemical equilibrium. However, there are difficulties in studying water-uptake kinetics through laboratory measurements. In the absence of chemical reaction, the flux of water molecules transferred from vapor into the liquid phase is governed by the mass accommodation coefficient, which is defined as the fraction of molecules colliding with the surface that enter the liquid phase. A direct measurement of water uptake will yield values that include additional effects of localized diffusion and partitioning of vapor molecules [*Li et al.*, 2001], which must be estimated a posteriori. Therefore, experimental values of inferred mass accommodation of water vapor into water alone vary by three orders of magnitude [*Marek and Straub*, 2001]. The picture of water uptake becomes additionally complex when coated by an organic film, which can change rates of diffusion, evaporation, and mass accommodation simultaneously.

[3] Simulations report that retardation in rate of water uptake due to organic films may be sufficient to alter cloud droplet size spectrum and number concentrations even if equilibrium water uptake is unchanged [*Chuang et al.*, 1997; *Feingold and Chuang*, 2002; *Medina and Nenes*, 2004]. The mechanism by which such rate reductions occur for some organic components is not well established [*Donaldson and Vaida*, 2006], as changes in diffusion coefficients would be too rapid to explain observed delays of seconds or longer [*Chan and Chan*, 2007]. *Chakraborty and Zachariah* [2008] simulated hydrophobic organic compound surrogates coating a 4 nm aqueous droplet and found that such coatings can reduce sticking probabilities of water vapor on particles to 11–16% with respect to vapor molecules impinging on a pure aqueous droplet, which may partially explain reduction in overall water uptake rates. The accurate prediction of water uptake rates for a variety of particle composition and morphology are important for design and operation of aerosol instrumentation [*Chan and Chan*, 2005; *Ruehl et al.*, 2008] and estimating the aerosol indirect effect [*Feingold and Chuang*, 2002]. *Shantz et al.* [2010] report that inhibition of water uptake by organic films can increase the number of cloud droplets compared to the base case where the film is not present.

[1]Scripps Institution of Oceanography, University of California, San Diego, La Jolla, California, USA.

0148-0227/11/2010JD014842

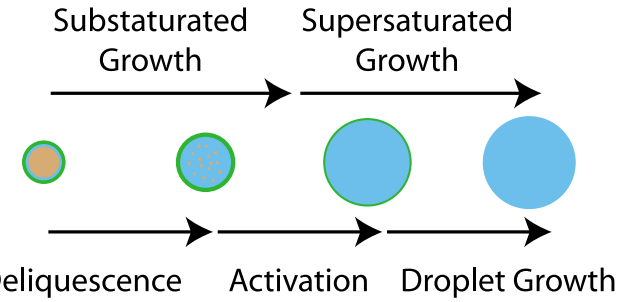

Figure 1. Idealized hygroscopic growth of aerosol coated by organic film. Brown represents solute, blue represents water, and green represents organic film, and these are meant to illustrate relative proportions of components.

[4] Surface-active organic compounds comprising an organic film may be broadly categorized into soluble and insoluble species; in the case of monomolecular, monolayer films, these are often referred to as Gibbs and Langmuir films, respectively [*Melzer et al.*, 1998]. The interphase transport of water molecules between an aqueous subphase and the vapor phase may be influenced by a large number of molecular properties of the film, including chain length, polar head group, acidity, solubility, charge, and molecular orientation [*Donaldson and Vaida*, 2006]. H. Tervahattu and coworkers have observed biogenic fatty acid (e.g., palmitic, myristic, stearic acids) coatings on sea salt aerosols [*Tervahattu and Juhanoja*, 2002] and continental sulfate aerosols [*Tervahattu et al.*, 2005] using time-of-flight secondary ion mass spectrometry. Single-particle measurements of organic functional groups with X-ray microscopy (STXM-NEXAFS) provide evidence of organic acid layers in dried CCN-sized particles [*Russell et al.*, 2002; *Takahama et al.*, 2010]. In addition, fatty acid compounds likely to be found as surface-active coatings have been measured by numerous bulk measurements, comprising up to 70% of the characterized organic mass [e.g., *Rogge et al.*, 1993; *Schauer et al.*, 1999; *Cheng et al.*, 2004].

[5] The mass accommodation of various vapor molecules onto equally wide variety of surfaces, also often referred to as the condensation coefficient in the case that vapor and condensed phase composition are molecularly identical, have been mechanistically studied through molecular dynamics (MD) simulations. The MD approach assumes a representation of atoms and molecules, based in classical mechanics, interacting through force field potentials. The equations of motion are solved numerically while interatomic interactions are evaluated at each iteration. Molecular dynamics has been used to estimate mass accommodation coefficients of vapor phase molecules onto "slabs" of solvent, with algorithms driven by thermodynamic perturbation and transition state theory [*Taylor et al.*, 1997; *Nagayama and Tsuruta*, 2003], equilibrium evaporation rates in vacuum [*Matsumoto and Kataoka*, 1994; *Ishiyama et al.*, 2004], and direct simulation of scattering events [e.g., *Wilson and Pohorille*, 1997; *Morita et al.*, 2004; *Tsuruta and Nagayama*, 2004; *Vieceli et al.*, 2004; *Chakraborty and Zachariah*, 2008] (and also discussed in reviews by *Garrett et al.* [2006], and *Morita and Garrett* [2008]). *Bahadur and Russell* [2008] additionally illustrate the use of molecular dynamics simulations to assess the relative contributions of gas phase diffusion and mass accommodation to net water uptake by a NaCl nanoparticle during the onset of deliquescence.

[6] We simulate water vapor molecules impinging on aqueous and monolayer-coated aqueous surfaces with molecular dynamics simulations to investigate how the presence of organic films affects the mass accommodation behavior of water vapor on condensed phase water. The mass accommodation behavior of the CCN-active particle will change during the course of deliquescence and subsaturated water uptake, and cloud-droplet growth in supersaturated conditions (Figure 1), during which both the surface concentration and subphase composition will vary. From a large domain of possible candidate molecules, surface concentrations, aqueous subphase composition, we initiate this investigation by selecting an eight-carbon amphiphile (octanoic, or caprylic acid) at 29 and 18 $Å^2$ per molecule densities and a 14-carbon amphiphile (myristic, or tetradecanoic acid) at a 29 $Å^2$ per molecule coverage. Octanoic and myristic acids have previously been used in the laboratory to represent film-forming or insoluble organic compounds in atmospheric aerosols [e.g., *Hansson et al.*, 1998; *Raymond and Pandis*, 2002; *Chan and Chan*, 2005]. Both of these molecules contain a carboxylic acid head group and a hydrocarbon tail and are positioned to form a monolayer film over a slab of water molecules, which can correspond to an idealized composition of a wet aerosol or growing cloud droplet coated by a thin organic film. The geometry of a slab is used to represent a section of a solution-air interface in an aerosol or cloud drop that is large enough that surface curvature effects are minimal. For pure droplets of water, this condition applies to ones with diameters larger than 50 nm [*Seinfeld and Pandis*, 2006]. As this work reports the results of a computer experiments, our use of the term "observation" will refer in this context to the outcomes of the simulated molecule trajectories.

2. Methods

2.1. Molecular Geometry and Potential Specification

[7] We use potentials, charges, and geometry for TIP4P-Ew water molecules as specified by *Horn et al.* [2005]. The initial geometry for organic molecules is taken from 3-D `sdf` files archived in the National Institutes of Health PubChem database. The organic molecules are simulated with their carboxylic acid head groups in protonated form. The pK_as of octanoic acid and myristic acid are effectively 5.9 [*Garner and Behal*, 1975] and 7.9 [*Heikkila et al.*, 1970], respectively, and aerosols and cloud or raindroplets are generally acidic. The exact pH can vary depending on composition, but cloud, rain, and fogwater have reported acidities between pH 2 and 5 [*Seinfeld and Pandis*, 2006], pH 2–5 for marine aerosol [*Keene et al.*, 2004], and pH 1–4 for (submicron) urban aerosol [e.g., *Zhang et al.*, 2007]; observations of more acidic aerosols have been reported in rural areas [*Liu et al.*, 1996]. Therefore, under these conditions most of the acid groups should be protonated. The OpenBabel software package is used to convert sdf files to mol2 format, which is processed by antechamber [*Wang et al.*, 2006] for atom and bond-type perception and partial charge calculations by the AM1-BCC method [*Jakalian et al.*, 2000]. The mol2 file provides an enumeration

of atoms (vertices) and bonds (edges), which are used to find the angle and dihedral constraints for the organic molecule (Appendix A). We use the Generalized AMBER Force Fields (GAFF) [*Wang et al.*, 2004] for specification of constraint parameters for intramolecular bonds, angles, and dihedrals, and intermolecular van der Waals interactions. GAFF has been shown to adequately reproduce properties of lipid bilayers [e.g., *Siu et al.*, 2008].

2.2. Initialization of Water Slab and Organic Monolayer Coating

[8] The water slab is generated by translating a single TIP4P-Ew water molecule into an fcc lattice configuration. Two blocks were generated: one with 864 molecules in a 30 × 30 × 100 Å^3 box, and another with 1440 molecules in a 38 × 38 × 145 Å^3 box, so that both slabs are approximately ~40 Å thick. The slab containing 864 molecules is equilibriated for 2.75 ns. Organic molecules are added to the surface of the slab containing 1440 water molecules after 100 ps and then equilibriated out to 2.75 ns. Surface tension and density estimates generally converged within range of reported values after approximately 1 ns of equilibration for each slab. When "attaching" organic molecules to the surface of the slab, we specify the initial positions of organic molecules to minimize van der Waals repulsion at the aqueous surface to reduce losses of organic molecules to the void space. Let r^* = the minimum of the Lennard-Jones (LJ) well between a pair of atoms, (x, y, z, a) the 3-D coordinates and type a of an atom belonging to a water molecule, and (x', y', z', a') the 3-D coordinates and type a' of an atom belonging to an organic molecule. For any fixed (x', y') position of an atom from an organic molecule, the z' coordinate corresponding to the minimum in LJ potential between any two atoms (a and a') is

$$z_{atom} = f_{z'}\left(x', y', x, y, z, r^*_{a'-a}\right) = z + r^*_{a'-a}\cos\sin^{-1}\left(\frac{x'-x}{r^*_{a'-a}\cos\tan^{-1}\frac{y'-y}{x'-x}}\right).$$

The distance corresponding to the maximum z' for any a' and a combination is the most desirable with respect to minimization of repulsion due to LJ forces. Electrostatic interactions are neglected in this calculation but may be considered for a full geometry optimizations, but the algorithm described by equation (2) was adequate to prevent detachment of organic molecules in our case. Given the sets of atoms in each organic molecule and water slab (O and W, respectively), the optimal z' position for the organic molecule is

$$z_{molecule} = \max\left\{ f_{z_i'}\left(x_i', y_i', x_j, y_j, z_j, r^*_{a_i'-a_j}\right) \middle| (i,j) \in O \times W \right\}.$$

This algorithm is used to attach 49 molecules of octanoic acid or myristic acid in a 7 × 7 molecule^2 grid to the surface of the water cube comprising 1440 molecules. Two octanoic acid-coated slabs are examined: one at a surface density of 29 Å^2 per molecule, and another at 18 Å^2 per molecule. The latter is generated by compressing the original octanoic acid coated slab, removing all but 864 water molecules, and subjecting to an additional 2.75 ns equilibration routine.

2.3. Calculation of Bulk and Interfacial Properties

[9] The bulk density is calculated from the number of organic molecules per volume in the bulk of the slab. The order parameter for the octanoic acid chains are calculated as an ensemble average of the $z'z'$ component of the order-parameter tensor ($\underline{\underline{S}}$) for the nth carbon atom [*Tieleman et al.*, 1997]

$$(S_{z'z'})_n = \frac{1}{2}\left\langle 3\cos^2(\theta_{z'}) - 1 \right\rangle_n.$$

$\theta_{z'}$ is the angle between "molecular axis" (a hypothetical line segment adjoining two neighboring carbon atoms) and the vector normal to the monolayer surface, which is calculated as the scalar product of the $C_{n-1} - C_{n+1}$ vector and the unit vector in the positive z direction.

[10] Coverage of the slab surface by the organic molecules is expressed as a fraction, computed from a convex hull analysis. A minimum convex set (convex hull) enclosing the carbon atoms in the hydrocarbon backbone of the fatty acids projected onto x-y space is used to calculate the spatial area covered by the film for any slab and divided by the total area of the slab along the same dimensions. This calculation was repeated for 20 states (20 different time steps) for each system to capture the variability in these estimates.

2.4. Simulation of Impinging Events

[11] A single molecule of water placed at a height z and position (x, y) is directed toward the slab with velocity v, and one of several events is recorded: {absorption, adsorption, scattering, desorption, entrainment}. These classifications are based on categories introduced by *Matsumoto* [1998], *Ishiyama et al.* [2004], and *Roeselová et al.* [2003], with the addition of a phenomenon (entrainment) observed only for cases in which an organic film is present. We differentiate impinging molecules incorporated at the film-water interface and those that are trapped in the monolayer by classifying them as being in an adorbed and entrained state, respectively. Fifty samples are drawn from equal probability intervals generated in uniform (x, y) coordinate-space and Boltzmann distribution for velocity (for T = 300 K), and impinged upon one of two slabs sampled from different time intervals between 1 and 2.75 ns, for a total of 100 impinging events for each type of surface. The temperature used here is chosen to compare with previous simulations of water mass accommodation and to provide a conservative estimate of the influence of the organic film. The initial z position is 15 Å above the top of the water slab or film. The mass accommodation coefficient is generated from an accounting of the observed events [*Roeselová et al.*, 2003; *Vieceli et al.*, 2005]:

$$\alpha' = \frac{n_{absorb} + \lfloor p_k n_{adsorb} \rceil + \lfloor p_{k(2)} n_{entrain} \rceil}{n_{impinge}}, \quad (1)$$

where

$$p_k = 1 - \frac{n_{desorb}}{n_{absorb} + n_{entrain} + n_{desorb}},$$

$$p_{k(2)} = 1 - \frac{n_{desorb}}{n_{absorb} + n_{adsorb} + n_{desorb}},$$

$$n_{impinge} = n_{absorb} + n_{adsorb} + n_{desorb} + n_{scatter} + n_{entrain}.$$

n_i is number of observations of event i, and α' is the sticking probability which we use to quantify mass accommodation; the enclosures denote the nearest-integer approximation; p_k is a correction factor which reduces the adsorbed number of molecules to account for the number of molecules expected to desorb beyond the duration of simulation; and $p_{k(2)}$ is a similar correction factor for molecules entrained or adsorbed in the monolayer. *Wilson and Pohorille* [1997] originally proposed a modification to the number of surface-absorbed states using a transition state theory expression, but *Vieceli et al.* [2005] proposed an alternative method of calculation that bounds the correction factor to physically realistic values lying in the interval between 0 and 1. We adapt the latter method for the calculation of p_k and $p_{k(2)}$ in this work. For this purpose, molecules are considered to be in a self-adsorbed or entrained state when the molecules remain in the respective layers longer than the time required to reach thermal equilibrium.

[12] As the results of these simulations can be interpreted as binary outcomes of "sticking" or "not sticking" from a limited number of trials, we can examine our uncertainty in this coefficient by considering our observations as a binomial random variable (with correction for possible desorption and subsequent approximation to the nearest integer). The limits of the confidence interval in reported mass accommodation coefficient is expressed as an exact binomial confidence interval [*Clopper and Pearson*, 1934]:

$$\left[\left\{\alpha_l' \middle| \sum_{k=x}^{n}\binom{n}{k}\alpha_l'^{k}(1-\alpha_l')^{n-k} = a/2\right\},\ \left\{\alpha_u' \middle| \sum_{k=0}^{x}\binom{n}{k}\alpha_u'^{k}(1-\alpha_u')^{n-k} = a/2\right\}\right]; \quad (2)$$

α' is the mass accommodation coefficient as described by equation (1), with subscripts l and u denoting the lower and upper bounds, respectively; n is the total number of trials and k is the number of successes (i.e., number of molecules sticking to the surface); $\binom{n}{k}$ is the binomial coefficient; and a is the significance level, which is chosen to be 0.05 (corresponding to a 95% confidence interval).

2.5. Simulations Parameters

[13] DL_POLY 2.18 [*Smith et al.*, 2002] compiled for parallel and single-node architectures is used for the simulations. A 1.0 fs time step is used in all cases. Slabs and coated slabs are equilibriated in NVT ensemble with the Nose-Hoover thermostat [*Evans and Holian*, 1985], but run in the NVE ensemble to prevent velocity rescaling. An NVT ensemble is selected as the nominal ensemble for equilibration as it represents an analog to Langmuir troughs used for the study of films [*Baoukina et al.*, 2009] in other atmospherically relevant experiments [e.g., *Cosman and Bertram*, 2008], and the surface structure of these films in atmospheric particles and droplets will be constrained by the surface area and concentration of the organic molecules (which is simulated by maintaining a constant area in the horizontal dimensions). The Velocity Verlet algorithm is used for time integration, and SHAKE [*Ryckaert et al.*, 1977] is used to maintain rigid body constraints (bond lengths and angles) for the water molecules. Orthorhombic periodic boundary conditions are used, and long-range Coulombic interactions are handled by the smooth particle mesh Ewald algorithm [*Essmann et al.*, 1995]. The cutoff radius for van der Waals interactions is set to 13 Å [*Vega and de Miguel*, 2007].

3. Results and Discussion

3.1. Equilibriated Slab Properties

[14] The bulk density of pure water slab is estimated to be 0.992 g/cm^3, and for water in the coated slab the bulk density is estimated to be 0.996 g/cm^3, which are values expected for water [*Vega and de Miguel*, 2007]. The surface tension was also computed from integrating the difference between normal and vertical pressure tensor components: $\gamma_T = \int[P_N - P_L]dz = L_N(\overline{P}_N - \overline{P}_L)$, where γ_T is the total interfacial tension in the system, P_N is the normal component and is taken to be the σ_{zz} pressure tensor component, and P_L is the lateral pressure and is computed to be $(\sigma_{xx} + \sigma_{yy})/2$. The surface tension of each void-liquid interface in the pure water case (γ_w) is computed as $\gamma_T/2$, due to symmetry. This value is 66 mN/m, as reported by *Vega and de Miguel* [2007] for the same TIP4P-Ew potential set, which is 6 mN/m lower than the measured value at T = 300 K (CRC Handbook). Classical mechanical simulations of water are known to slightly underreport surface tensions in comparison to measurements [*Duncan and Larson*, 2008]. For the slab coated with the monolayer, the surface tension of monolayer (γ_m) is computed as $\gamma_T - \gamma_w$. The values calculated for γ_m are 38 mN/m, 56 mN/m, and 103 mN/m for the octanoic acid monolayer (29 Å^2/molecule), compressed octanoic acid monolayer (18 Å^2/molecule), and myristic acid monolayer (29 Å^2/molecule), respectively. The reduction in interfacial tension from 66 to 38 mN/m by the octanoic acid monolayer with an area per molecule of 29 Å^2 is in agreement with measurements (31 mN/m at 20°C by *Neys and Joos* [1998]). The estimated value for the 18 Å^2/molecule octanoic acid monolayer is unexpectedly high, considering that surface tensions normally decrease with decreasing area per molecule [e.g., *Kaganer et al.*, 1999]. An increase is expected, however, for collapsing monolayers [*Baoukina et al.*, 2007], as much as 30 mN/m for stearic acid on pure water [*Kundu and Langevin*, 2008], and undulations at the interface present in the 18 Å monolayer case suggests that this film may be captured in a state near the threshold prior to collapse (further discussed below). The value of surface tension calculated for myristic acidis much higher compared to measurements (51 mN/m at 20°C [*Langevin and Griesmar*, 1980]). Possible impact of these discrepancies on the impinging simulation will be discussed in section 3.2.

[15] The order parameter for an organic molecule is a measure of the average spatial restriction of methyl units, indicating tilt angles and transgauche distribution of chain units [*Tieleman et al.*, 1997]. The values for the order parameter can range between −0.5 and 1, with a pair of bond segments perpendicular to the interface assuming an order parameter of unity and one laying flat in the plane of the surface equal to −0.5. Our calculated order parameter profiles (Figure 2) indicate that the myristic acid and 18 Å^2/molecule octanoic acid are straighter than the octanoic acid

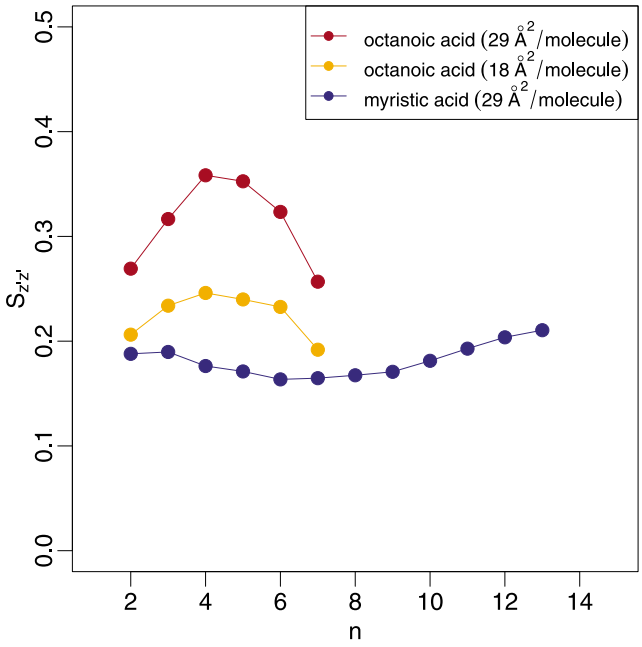

Figure 2. Order parameters of the monolayers.

at 29 Å^2/molecule (Figure 3a), supported by the near-uniform values in order parameter, but existing at a tilted angle, as evidenced by the departure in average order parameter from unity. Langmuir monolayers are known to undergo two-dimensional phase transitions across a range of surface pressures, from gas to liquid (expanded and condensed states, LE and LC, respectively) and then a solid phase, before collapsing to create three-dimensional structures [*Kaganer et al.*, 1999]. The order parameters here exhibit characteristics of LE (29 Å^2/molecule octanoic acid) in which the molecules are relatively disordered, and LC films (29 Å^2/molecule myristic acid) in which organized structures ("tilted condensed" [*Kaganer et al.*, 1999]) are seen to emerge in the surface phase. Additionally, ripples or undulations appearing at the monolayer interface for the 18 Å^2 octanoic acid film (Figure 3b) suggests a state verging on the onset of collapse. Published pressure area isotherms for octanoic acid extend down only to about 28 Å^2, but rough extrapolations from *Neys and Joos* [1998] indicate that area per molecule corresponding to an approximate "equilibrium surface pressure" (ESP) estimated from *Seidl* [2000] indicate the area coverage below which the octanoic acid monolayer would show indications of collapse are approximately 25 Å^2. So the film is likely to be in or on the verge of a collapsed state at 18 Å^2 as stated, though no new phases are observed to form in the bulk or on the surface in our simulations; however, this may be a limitation of low germ nucleation rates and extremely low sample size to recreate such an event. Calculation of the surface tension and bulk density over the last 1.5 ns of the 2.75 ns of initial equilibration indicates that the bulk slab density nor the surface energies at the monolayer interface were changing significantly. Even if the system is in a kinetically trapped, or metastable state, however, the system may be relevant for atmospheric applications. *Seidl* [2000] suggests that films in raindrops were found in an overcompressed state but not

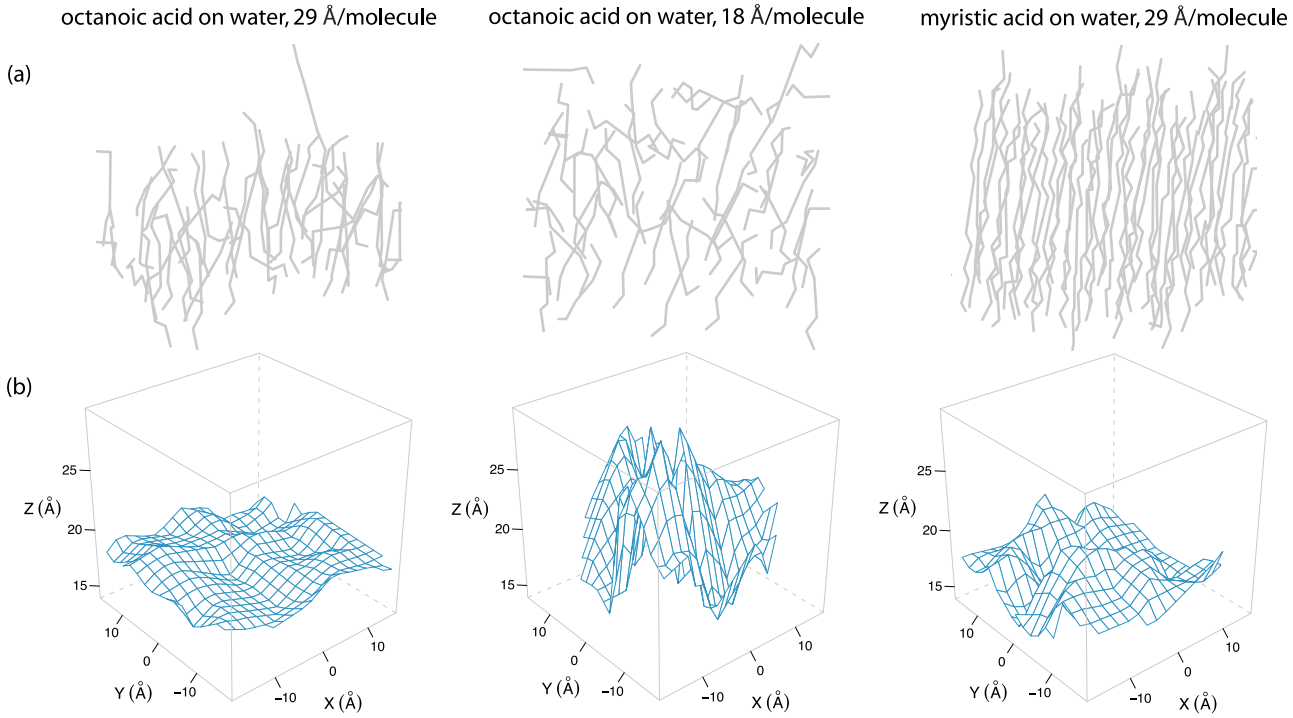

Figure 3. Characterization of equilibriated slabs. (a) Line representations of carbon backbones in organic films projected in *x*-*z* space. (b) Surfaces fitted to positions of carbon atom of carboxylic acid head groups. The wire frame surfaces are created by adjoining two-dimensional polygons defined by their vertices (carbon atoms) in three-dimensional space [*R Development Core Team*, 2010].

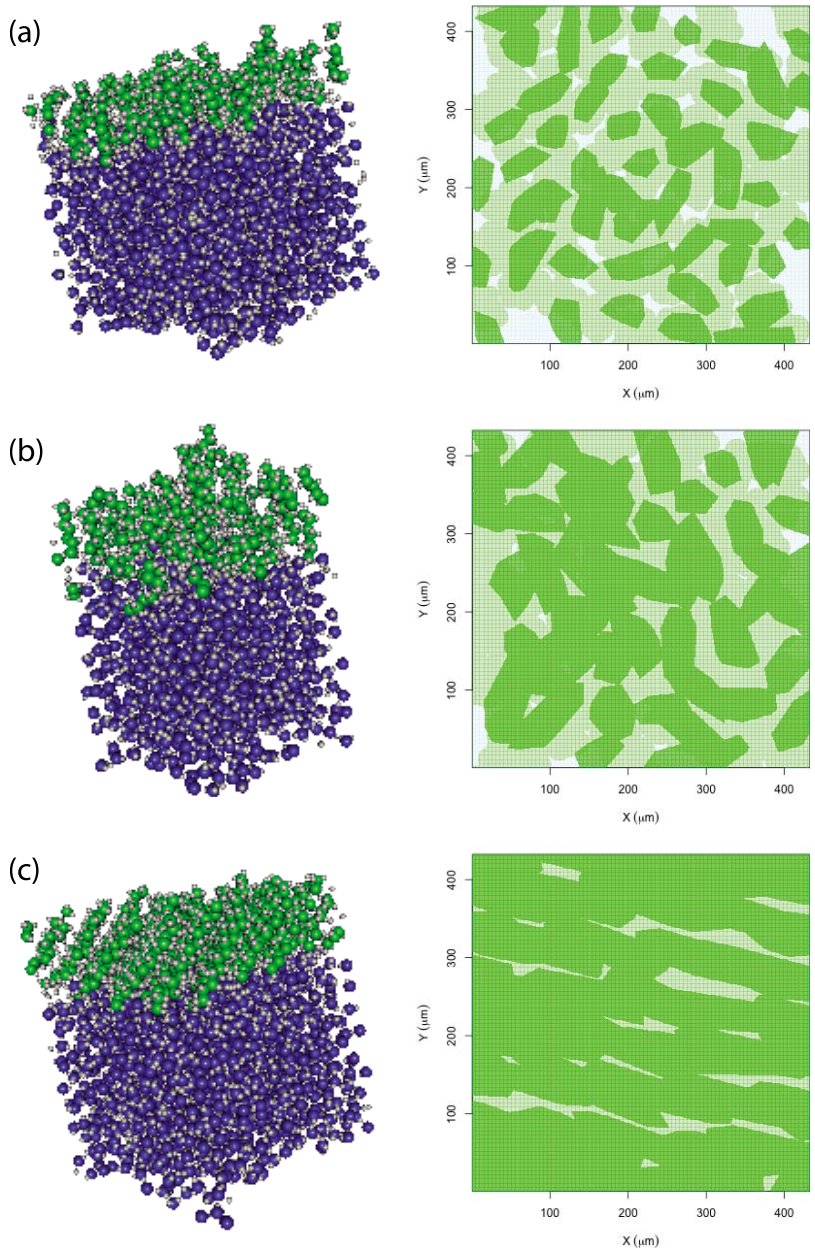

Figure 4. (left) Water slabs coated by (a) octanoic acid (29 $Å^2$/molecule), (b) octanoic acid (18 $Å^2$/molecule), and (c) myristic acid (29 $Å^2$/molecule). (right) Examples of convex hulls (dark green) enclosing amphiphile carbon backbones projected on *x*-*y* space, normal to direction of impinging water vapor molecule. Light green areas show projected van der Waal radii, which are shown for reference but are not used for calculation of projected area coverage of organic molecules.

having formed new phases. Furthermore, metastable states, particularly with regards to the nucleation of new phases (e.g., aerosols remain hydrated well below the thermodynamic deliquescence point [*Martin*, 2000]), are often found in the atmosphere as they may be relatively stable with respect to cloud condensation nuclei lifetimes (7 days on average [*Adams and Seinfeld*, 2003]), water condensation to and evaporation from aerosols in an updraft (5–100 s [*Chuang*, 2003]), or lifetimes of cloud droplet (~20 min [*Desboeufs et al.*, 2003]).

[16] The fraction of surface space occupied by the organic molecules on each slab, as determined by convex hull analysis, varied between 0.5 and 0.9 and increased monotonically from octanoic acid at 29 $Å^2$ per molecule surface coverage, octanoic acid at 18 $Å^2$ per molecule coverage, and myristic acid at 29 $Å^2$ per molecule coverage (Figure 4). This property is related to the mass accommodation coefficient in section 3.2. As these calculations neglect the contribution of the hydrogen atom and van der Waals radii,

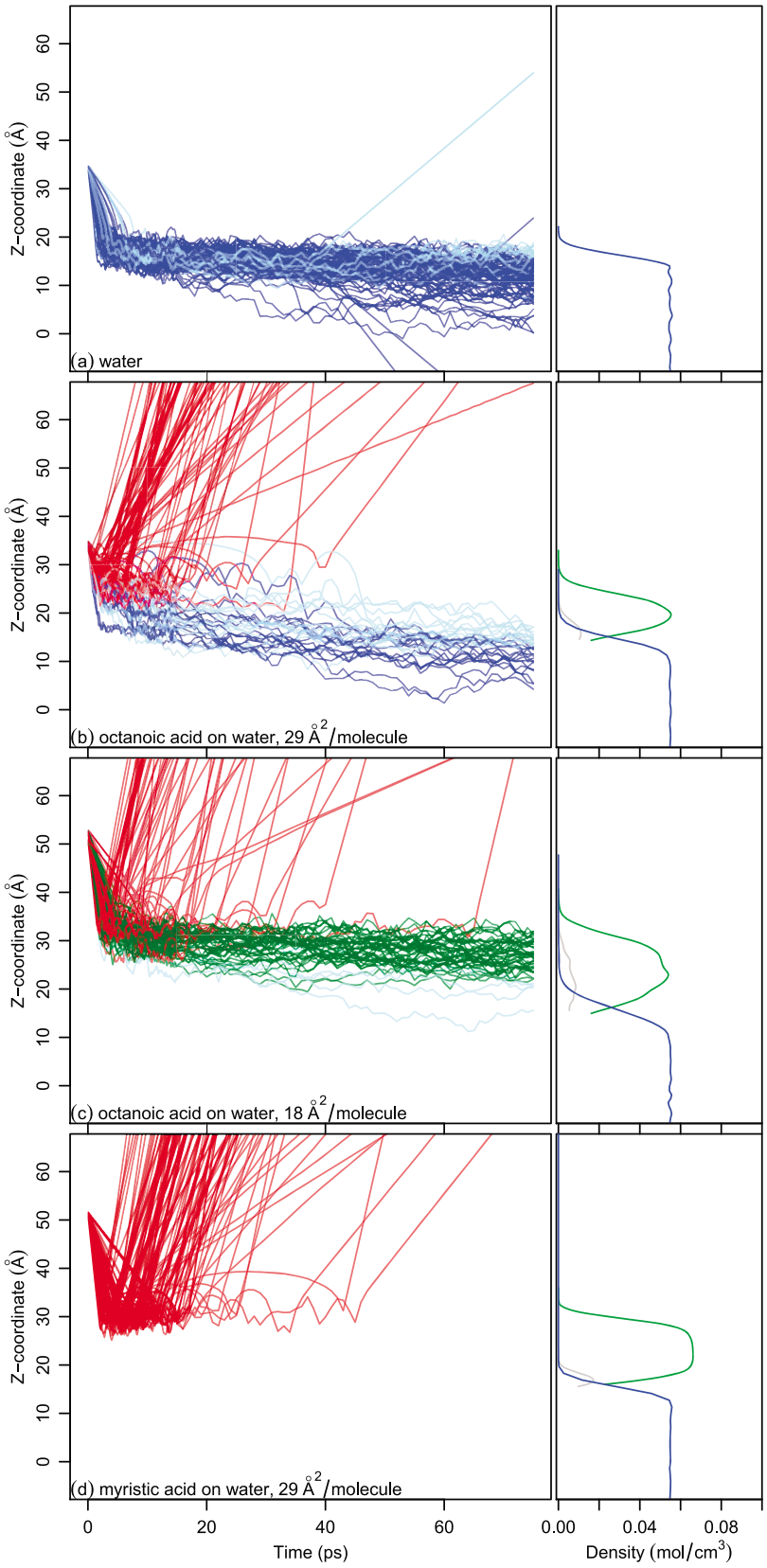

Figure 5. (left) Trajectories of impinging water molecule and estimated mass accommodation coefficients. (a–d) Z coordinate of oxygen atoms of water molecule impinging on water slab or film-coated slab. Colors indicate classification of impinging event outcomes: adsorbed (light blue), absorbed (dark blue), scattered (red), and entrained (dark green). (right) Profiles indicate number density of carbon (green), organic oxygen (gray), and aqueous oxygen (blue) atoms for each slab.

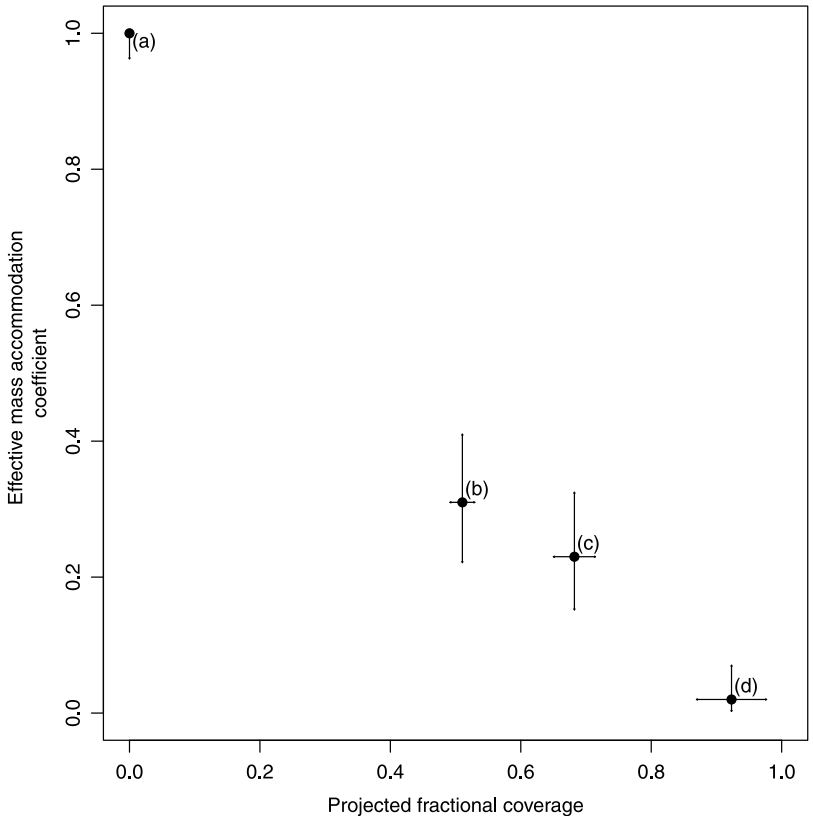

Figure 6. Estimated mass accommodation coefficients with two-sided confidence intervals (0.05 at the significance level) calculated from equation (2) and projected area from convex hull analysis. Letters next to symbols correspond to slabs indicated in Figure 5: a is pure water, b is octanoic acid on water (29 $Å^2$/molecule), c is octanoic acid on water (18 $Å^2$/molecule), and d is myristic acid on water (29 $Å^2$/molecule).

they are meant only to capture qualitative trends in surface coverage.

3.2. Mass Accommodation

[17] The estimated mass accommodation coefficient for water vapor on a pure water surface is estimated to be 1.0 [0.96, 1.0] (values in brackets indicate range of binomial confidence interval). Illustrations of individual vapor phase trajectories are shown in Figure 5. The value of unity for the pure water coefficient is consistent with those reported by similar molecular dynamics simulations by *Morita et al.* [2004] (at 273 K with SPC/E water potential), *Vieceli et al.* [2004] (at 300 K with POL3 water potential), *Tsuruta and Nagayama* [2004] (at 330 K with SPC/E water potential), and *Chakraborty and Zachariah* [2008] (at 300 K with SPC/E water potential)]. *Chakraborty and Zachariah* [2008] also report sticking probabilities between 0.11 and 0.16 for approximately 15 $Å^2$ per molecule coverage of fatty (dodecanoic C_{12}) acid on a 4 nm droplet of water (at $T = 300$ K with SPC/E water potential and LJ organic potential), which corresponds to a more densely packed surface than investigated in our simulations. The reduction in mass accommodation is seen for the case of water vapor molecules impinging on other surfaces examined: 0.30 [0.21, 0.40] for the surface covered by the 29 $Å^2$/molecule octanoic acid monolayer, 0.21 [0.13, 0.30] for the more densely packed 18 $Å^2$/molecule octanoic acid monolayer, and 0.0 [0.0, 0.04] myristic acid monolayer (Figure 6). No correlation between the trajectory classification with initial position or velocity of the impinging molecule was observed. The nondesorbing probability from an adsorbed state (p_k) was 1.0 for water and 29 $Å^2$/molecule octanoic slab, and the correction factor ($p_{k(2)}$) for the entrained state was 0.44 for the 18 $Å^2$/molecule octanoic acid slab case. These correction factors were calculated by determining the outcome of particles that had achieved a state of surface adsorption or entrainment according to thermal equilibrium. Times to reach thermal equilibrium were estimated to be on the order of 10 ps (Figure 7) for molecules adsorbed into the water surface (pure water slab) and those entrained in the film (18 $Å^2$/molecule octanoic acid slab).

[18] The change in accommodation behavior can occur through direct interaction of the water molecule with the film itself, or a change in the properties of water at the interface. Since the effective mass of the organic molecule is far greater than the water molecule (molecular weight of 144.21 or 228.37 versus 18.01), an inelastic collision is likely to result in the reflection of the smaller water molecule if we interpret the results from a momentum-conservation argument for colliding particles [*Clement et al.*, 1996]. The impinging molecule will transfer energy to the substrate through its additional (rotational) degrees of freedom [*Clement et al.*, 1996] only as permitted by the number and of interactions. The probability of scattering is largely

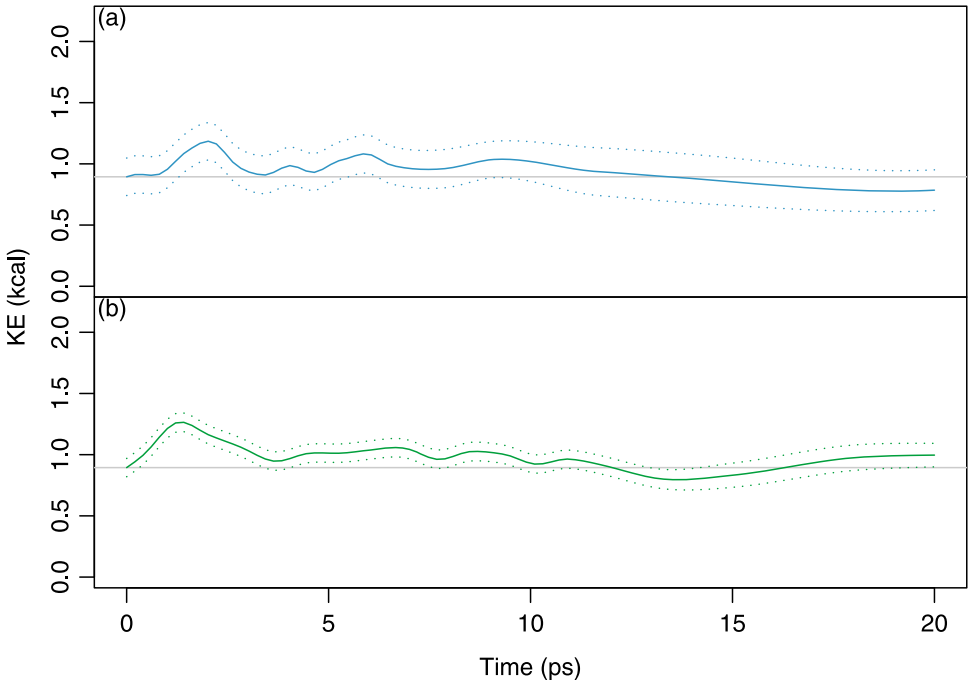

Figure 7. Time series of kinetic energies for (a) adsorbed water molecules on water slab and (b) entrained water molecules in 18 Å^2/molecule octanoic acid-coated water slab. Horizontal lines correspond to the average total kinetic energy [*Wilson and Pohorille*, 1997], and light blue and green are local regression fits [*Loader*, 1999] to the kinetic energy of impinging water molecules. Dotted lines indicate 95% confidence bands as estimated by local regression.

determined by reflection of water molecules from the hydrophobic chain of the fatty acids, except in the case that they become entrained in the matrix of the monolayer film as observed for the case of the 18 Å^2/molecule octanoic acid monolayer. The simulations in which the impinging water molecules became entrained within the monolayer were extended for an additional 125 ps (to 200 ps), with no observable change in state. Studies have previously reported instances of organic films effectively acting as a solvent for other gas phase molecules [e.g., *Mmereki et al.*, 2003]. The pair radial distribution functions between the oxygen atom of the entrained water molecule and atoms of the octanoic acid indicate that the water molecules preferentially lie near the hydrophilic head group of the amphiphile, which suggests an explanation for its apparent preference for adsorption rather than desorption (Figure 8).

[19] The interfacial surface tension represents the balance of interfacial energy as it is estimated from the pressure tensor, which is in turn computed from the kinetic energy and molecular virial (or configurational energy [*Marc and McMillan*, 1985; *Allen and Tildesley*, 1990]. The average kinetic energy tensor should be isotropic and therefore negligible in the ideal case [*Lindahl and Edholm*, 2000], leaving the configurational interactions to regulate the interfacial energy and surface tension. For a monolayer film of amphiphiles coating an aqueous substrate, spatially resolved energy profiles indicate that the reduction in energy is located at the interface of water and the hydrophilic head group (as determined for a phospholipid membrane [*Baoukina et al.*, 2008]). As such, the discrepancy between simulated and expected surface tensions for the myristic acid monolayer may possibly affect the interaction energies and subsequently the reported mass accommodation estimate through errors in the calculated desorption/absorption probability of molecules adsorbed at the aqueous interface. However, *Archer and La Mer* [1955] report that mass transfer of water across fatty acid monolayers on a liquid substrate is independent of surface pressure. Furthermore, since much of the mass accommodation of the impinging molecules is regulated through direct interaction with the hydrocarbon tail and subsequent scattering events rather than desorption from an adsorbed state, the errors in estimates of mass accommodation coefficients from these discrepancies are perceived to be small.

[20] For theoretical prediction of water uptake by particles and growing cloud droplets in respective subsaturated and supersaturated vapor pressures, the parameter regulating incorporation of vapor phase molecules at the surface is the mass accommodation coefficient. Experiments which independently derive mass accommodation coefficients measure uptake coefficients, and mass accommodation is calculated after assuming contributions to diffusion and gas-liquid partitioning [*Li et al.*, 2001]. For pure water, recent estimates of mass accommodation coefficient reported by experiment and by impinging simulations range between 0.2 [*Li et al.*, 2001] and ≥0.99, with near-unity values reported from simulations [*Morita et al.*, 2004; *Vieceli et al.*, 2004; *Tsuruta and Nagayama*, 2004]. *Morita et al.* [2004] show that uncertainties in the diffusion process can lead to the mass accommodation values reported by droplet-train experiments. From the calculations reported here, less than 0.01 mass percent of a film-forming compound on a 100 μm

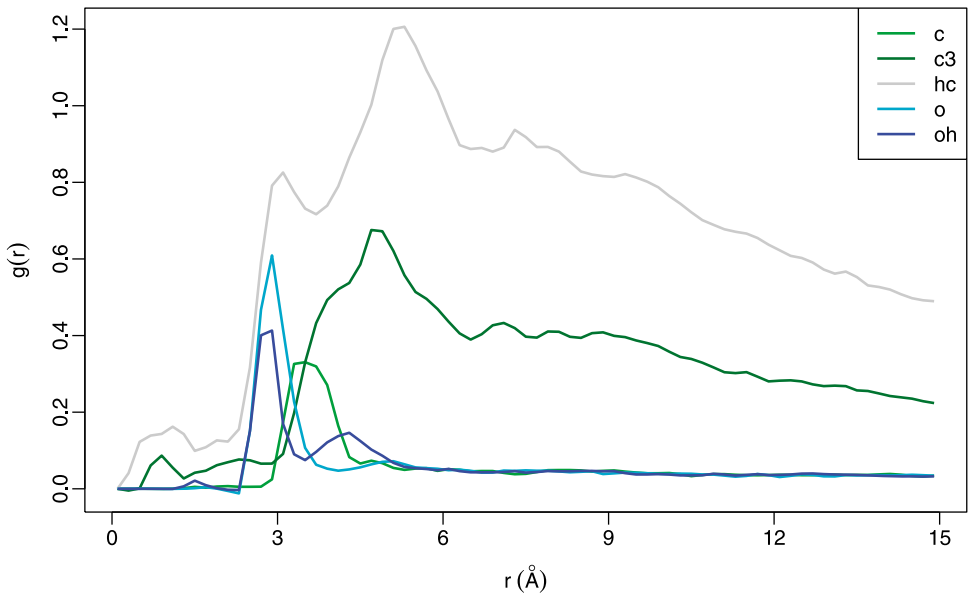

Figure 8. Radial distribution functions of oxygen atom of entrained water molecules and atoms in octanoic acid film (o, double-bonded oxygen of acid head group; oh, oxygen in hydroxyl group of acid head group; c, carbon atom in acid head group; c3, carbon atom in hydrocarbon tail; hc, hydrogen atom in hydrocarbon tail).

droplet can also reduce mass accommodation coefficient by 70% or more.

[21] In these simulations, the impinging molecule was directed normal to the interface of the coated and uncoated surface. Under the conditions in which entrainment of the water molecule into the organic monolayer is negligible (shown by simulations on octanoic acid (29 $Å^2$) and myristic acid (29 $Å^2$)), the reduction in mass accommodation by amphiphiles may largely be governed by area coverage (Figures 5b and 5d), as has been reported for evaporative fluxes [*Adamson*, 1990]. It is possible that the effective area of water exposed may be diminished for a molecule following a nonorthogonal trajectory, further reducing the apparent mass accommodation. This would be in contrast with estimation of condensation coefficients, where incident angle of the impinging molecule has been shown to play an insignificant role [*Tsuruta and Nagayama*, 2004]. Lower mass accommodation coefficients are also expected for lower temperatures [e.g., *Clement et al.*, 1996; *Tsuruta and Nagayama*, 2004]. The actual mass accommodation coefficient for the 18 $Å^2$/molecule octanoic acid may also be a high estimate as these simulations consider the accommodation of a single water molecule at a time. As more water molecules are entrained in the film matrix, the occupation of its available adsorption sites may follow the form of a Langmuir isotherm until saturation [*Ramaswami et al.*, 2005], beyond which more water molecules cannot be entrained.

[22] In this work, we considered the influence of relatively insoluble amphiphiles at low surface concentrations. *Feingold and Chuang* [2002] considered a constant (reduced) mass accommodation coefficient for organic films at mass concentrations between 2 and 10%; the area per molecule investigated here (18 and 29 $Å^2$) would correspond to even smaller mass fractions for typical cloud droplet sizes (Figures 9a and 9c). *Chuang* [2003] and *Ruehl et al.* [2008] report the prevalence of particles with even lower mass accommodation coefficients ($<10^{-1}$) from their field measurements. *Shantz et al.* [2010] reproduced observed growth of biogenically and anthropogenically influenced air masses with mass accommodation coefficients between 0.07 and 0.5, though subject to uncertainty in the equilibrium hygroscopicity of the particles. Organic acid coatings with thickness up to 0.6 μm have been observed in dried particles by X-ray microscopy [*Takahama et al.*, 2010]. In a limiting case, if all of this organic mass is assumed to remain partitioned to the surface in aqueous solutions upon hydration, these coatings would far exceed monolayer thicknesses. Figures 9b and 9d illustrate estimated film coverages from X-ray microscopy measurements extrapolated to cloud droplet sizes. Such coatings could possibly lead to such low mass accommodation coefficients under the assumption that scattering events dominate the interactions of water vapor molecules at the particle or droplet interface, as suggested by this study. However, the extent to which multilayers form at higher amphiphile concentrations is not certain, as the excess organic molecules break off from the surface and form micelles within the bulk aqueous volume beyond the formation of one or few monolayers [*Miller and Neogi*, 1985; *Baoukina et al.*, 2007].

[23] The scenarios for reduction in mass accommodation coefficients discussed above are notable, as *Chuang et al.* [1997] suggests that growth kinetics influence cloud formation for mass accommodation coefficients less than 0.1. The reduction in mass accommodation coefficient by a few mass percent of a C_{14} concentrated at the surface suggests that this condition can be prevalent in the atmosphere.

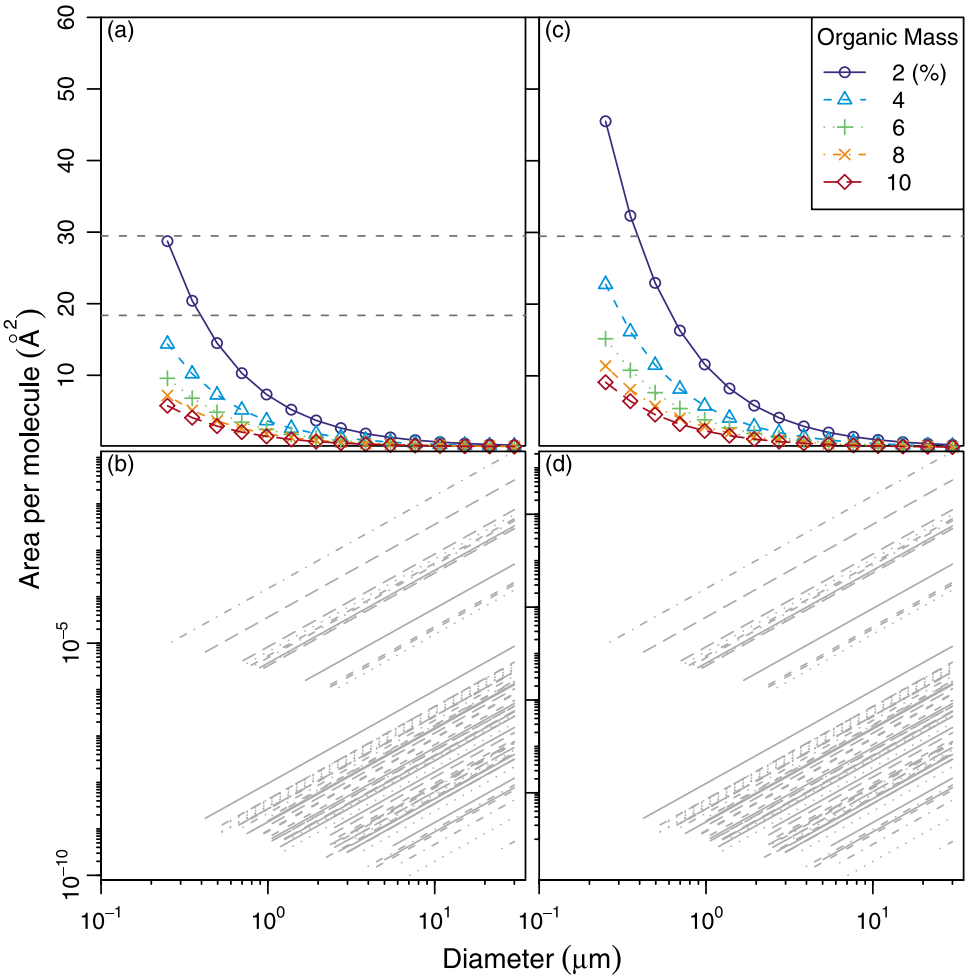

Figure 9. Coverages of organic films or layers as a function of particle/droplet diameter for assumed organic mass fractions (with molecular properties of (a) octanoic acid and (c) myristic acid) and coverages calculated from estimated coating thicknesses of carboxylic acids on individual particles from *Takahama et al.* [2010] (assuming molecular properties of (b) octanoic acid and (d) myristic acid). Dark, dashed gray horizontal lines in Figures 9a and 9c correspond to surface densities investigated in this work. Each line in Figures 9b and 9d extends from measured dry diameter and estimated film coverage of a particle by X-ray microscopy and is extrapolated to larger sizes assuming density of 1.0 g/cm^3 for the subphase and fixed number of molecules in the film.

However, there may be other scenarios in which other types of organic coatings permit more water molecules across the interface. Both *Chuang* [2003] and *Ruehl et al.* [2008] also report an increase in particle mass accommodation coefficients in the afternoon, and hypothesize that the organic compounds found in these particles are more hydrophilic in nature. Surface partitioning of such organic compounds may still occur if their presence exceeds the thermodynamic solubility limit in bulk solution, but such compounds at the surface generally form more porous films and present less of a barrier to interfacial transport of vapor molecules than do insoluble compounds [*Chuang*, 2003]. Shorter-chain acids are also reported to be more porous and permeable [*Torn and Nathanson*, 2002; *Gilman and Vaida*, 2006] to gases, as in the case of C_8 octanoic acid where the mass accommodation coefficient was not reduced by nearly as much as myristic acid. Partitioning of surface-active compounds into the bulk phase may also be of consideration, as this can reduce the concentration at the interface [*Sorjamaa et al.*, 2004; *Li et al.*, 2010]. Additionally, branched or unsaturated hydrocarbons may also reduce the packing efficiency [*Gilman and Vaida*, 2006; *Cosman and Bertram*, 2008] and lead to increased mass accommodation over the saturated, long-chain case. Mass accommodation may also be influenced by nonuniformity present in surface films. For instance, *Garland et al.* [2008] observed the formation of islands rather than uniform monolayers of oleic acid in the laboratory, and *Takahama et al.* [2010] reports the observation of nonuniform distribution of acid groups in ambient aerosols in a dry (helium) environment. Heterogeneities in surface structure may also have to be considered in addition to molecular composition of coating films when considering sticking probabilities. Further studies investigating the role of organic compounds on water mass accommodation are

desired for the generalization of the mass accommodation coefficient to a mass accommodation function, parameterized by film and subsurface properties.

4. Conclusions

[24] Molecular dynamics simulations were used to simulate impinging water vapor molecules on a slab of water and an slab of water coated by monomolecular organic films. TIP4P-Ew and Generalized AMBER Force Field potentials were selected to represent intermolecular and intramolecular interactions. The bulk density and surface tension of pure water, and the surface tension of water coated with octanoic acid at 29 Å^2/molecule were adequately reproduced. Surface tensions of the water coated by myristic acid (C_{14}) at 29 Å^2/molecule was higher than measurements, but the magnitude of errors introduced in the reported results of the mass accommodation estimate is expected to be small. Calculated order parameters and examination of surface structure indicate liquid-expanded and liquid-condensed states for the 29 Å^2/molecule octanoic acid and myristic acid films and a state at the onset of collapse for the 18 Å^2/molecule octanoic acid film.

[25] The mass accommodation coefficient of water vapor on pure water using a TIP4P-Ew potential is in agreement with values estimated using similar scattering methods but with other potentials for water (SPC/E [*Morita et al.*, 2004; *Chakraborty and Zachariah*, 2008], POL3 [*Vieceli et al.*, 2004]). Octanoic acid and myristic acid coatings with a coverage of 29 Å^2/molecule reduced the mass accommodation coefficient from 1.0 to 0.30 and 0.0, respectively, largely through the mechanism of scattering through interactions between the impinging water vapor molecule and the hydrocarbon tails. This reduction was to a first-order proportional with estimates of projected surface coverage of the hydrocarbon backbone of the amphiphiles. Our estimated mass accommodation coefficient of water vapor on a slab coated by these 8-chain and 14-chain fatty acids bounds the mass accommodation estimated by *Chakraborty and Zachariah* [2008] for a 12-chain fatty acid coating a 4 nm droplet in approximately twice the packing density at the surface. A notable case of mass accommodation was observed in which the impinging water molecule was entrained in the octanoic acid film with a coverage density of 18 Å^2. This surface structure showed undulations near the surface, indicating a monolayer nearing a state of collapse. The water vapor molecules entrained in this monolayer reached thermal equilibrium at a location just above the hydrophilic head group of the octanoic acid molecules, but within the layer of hydrocarbon tails.

[26] The three surfaces studied here show that scattering appears to be the main mechanism by which mass accommodation of water vapor is reduced, but the mechanism of "sticking" may depend on the compound, packing density, and resulting surface structure. Estimated reductions in mass accommodation coefficients resulting from less than 1% mass percent of monomolecular straight-chain fatty acid coatings on droplets >1 μm support the prevalence of extremely low mass accommodation coefficients measured during field campaigns. Mass accommodation can be influenced by surface concentration, molecule polarity, functionalization, chain length, degree of branching, and molecular heterogeneity, and these factors may be further considered in a refined effort at quantification. Surface heterogeneities or branched and unsaturated hydrocarbon tails may alternatively increase the mass accommodation coefficient; however, the temperature, low surface concentration, and orthogonality of initial trajectories used in our simulations are expected to provide a high estimate for mass accommodation of water vapor onto growing cloud droplets coated by straight-chain organic compounds.

Appendix A

[27] Given a molecular graph consisting of vertices (V) and edges (E), the set of angles are given by

$$\{(i,j,k) \in V^3 | [(i,j) \in E \wedge (j,i) \in E] \vee [(j,k) \in E \wedge (k,j) \in E] \vee i < k\},$$

and the set of dihedrals are similarly specified as

$$\{(i,j,k,l) \in V^4 | [(i,j) \in E \wedge (j,i) \in E] \vee [(j,k) \in E \wedge (k,j) \in E] \vee [(k,l) \in E \wedge (l,k) \in E] \vee i \neq k \vee j \neq l \vee j < k\}.$$

[28] **Acknowledgments.** The authors acknowledge NSF ATM-0904203 for funding, NSF TeraGrid and UCSD Triton Computing Resources for high-performance computing facilities, and Ranjit Bahadur for helpful suggestions.

References

Adams, P. J., and J. H. Seinfeld (2003), Disproportionate impact of particulate emissions on global cloud condensation nuclei concentrations, *Geophys. Res. Lett.*, *30*(5), 1239, doi:10.1029/2002GL016303.

Adamson, A. (1990), *Physical Chemistry of Surfaces*, Wiley-Interscience, New York.

Allen, M., and D. Tildesley (1990), *Computer Simulation of Liquids*, Oxford Univ. Press, New York.

Archer, R. J., and V. K. La Mer (1955), The rate of evaporation of water through fatty acid monolayers, *J. Phys. Chem.*, *59*, 200–208, doi:10.1021/j150525a002.

Bahadur, R., and L. M. Russell (2008), Water uptake coefficients and deliquescence of NaCl nanoparticles at atmospheric relative humidities from molecular dynamics simulations, *J. Chem. Phys.*, *129*(9), 094508, doi:10.1063/1.2971040.

Baoukina, S., L. Monticelli, S. J. Marrink, and D. P. Tieleman (2007), Pressure area isotherm of a lipid monolayer from molecular dynamics simulations, *Langmuir*, *23*, 12,617–12,623, doi:10.1021/la702286h.

Baoukina, S., L. Monticelli, H. J. Risselada, S. J. Marrink, and D. P. Tieleman (2008), The molecular mechanism of lipid monolayer collapse, *Proc. Natl. Acad. Sci. U. S. A.*, *105*(31), 10,803–10,808, doi:10.1073/pnas.0711563105.

Baoukina, S., S. Marrink, and D. Tieleman (2009), Structure and dynamics of lipid monolayers: Theory and applications, *Biomembrane Frontiers*, 75–99.

Chakraborty, P., and M. R. Zachariah (2008), Sticking coefficient and processing of water vapor on organic-coated nanoaerosols, *J. Phys. Chem. A*, *112*(5), 966–972, doi:10.1021/jp076442f.

Chan, M. N., and C. K. Chan (2005), Mass transfer effects in hygroscopic measurements of aerosol particles, *Atmos. Chem. Phys.*, *5*, 2703–2712, doi:10.5194/acp-5-2703-2005.

Chan, M. N., and C. K. Chan (2007), Mass transfer effects on the hygroscopic growth of ammonium sulfate particles with a water-insoluble coating, *Atmos. Environ.*, *41*(21), 4423–4433, doi:10.1016/j.atmosenv.2007.01.047.

Cheng, Y., S. M. Li, A. Leithead, P. C. Brickell, and W. R. Leaitch (2004), Characterizations of cis-pinonic acid and n-fatty acids on fine aerosols in the Lower Fraser Valley during Pacific 2001 Air Quality study, *Atmos. Environ.*, *38*(34), 5789–5800, doi:10.1016/j.atmosenv.2004.01.051.

Chuang, P. Y. (2003), Measurement of the timescale of hygroscopic growth for atmospheric aerosols, *J. Geophys. Res.*, *108*(D9), 4282, doi:10.1029/2002JD002757.

Chuang, P. Y., R. J. Charlson, and J. H. Seinfeld (1997), Kinetic limitations on droplet formation in clouds, *Nature*, *390*(6660), 594–596, doi:10.1038/37576.

Clement, C. F., M. Kulmala, and T. Vesala (1996), Theoretical consideration on sticking probabilities, *J. Aerosol Sci.*, *27*(6), 869–882, doi:10.1016/0021-8502(96)00032-8.

Clopper, C. J., and E. S. Pearson (1934), The use of confidence or fiducial limits illustrated in the case of the binomial, *Biometrika*, *26*, 404–413, doi:10.1093/biomet/26.4.404.

Cosman, L., and A. Bertram (2008), Reactive uptake of N_2O_5 on aqueous H2SO4 solutions coated with 1-component and 2-component monolayers, *J. Phys. Chem. A*, *112*(20), 4625–4635, doi:10.1021/jp8005469.

Desboeufs, K. V., R. Losno, and J. L. Colin (2003), Relationship between droplet pH and aerosol dissolution kinetics: Effect of incorporated aerosol particles on droplet pH during cloud processing, *J. Atmos. Chem.*, *46*(2), 159–172, doi:10.1023/A:1026011408748.

Donaldson, D. J., and V. Vaida (2006), The influence of organic films at the air-aqueous boundary on atmospheric processes, *Chem. Rev.*, *106*(4), 1445–1461, doi:10.1021/cr040367c.

Duncan, S. L., and R. G. Larson (2008), Comparing experimental and simulated pressure-area isotherms for DPPC, *Biophys. J.*, *94*(8), 2965–2986, doi:10.1529/biophysj.107.114215.

Essmann, U., L. Perera, M. Berkowitz, T. Darden, H. Lee, and L. Pedersen (1995), A smooth particle mesh Ewald method, *J. Chem. Phys.*, *103*(19), 8577–8593, doi:10.1063/1.470117.

Evans, D., and B. Holian (1985), The Nose–Hoover thermostat, *J. Chem. Phys.*, *83*, 4069–4074, doi:10.1063/1.449071.

Feingold, G., and P. Y. Chuang (2002), Analysis of the influence of film-forming compounds on droplet growth: Implications for cloud microphysical processes and climate, *J. Atmos. Sci.*, *59*(12), 2006–2018, doi:10.1175/1520-0469(2002)059<2006:AOTIOF>2.0.CO;2.

Garland, E., E. Rosen, L. Clarke, and T. Baer (2008), Structure of submonolayer oleic acid coverages on inorganic aerosol particles: Evidence of island formation, *Phys. Chem. Chem. Phys.*, *10*(21), 3156–3161, doi:10.1039/b718013f.

Garner, C. W., and F. J. Behal (1975), Effect of ph on substrate and inhibitor kinetic constants of human liver alanine aminopeptidase—Evidence for 2 ionizable active-center groups, *Biochemistry*, *14*(23), 5084–5088, doi:10.1021/bi00694a009.

Garrett, B. C., G. K. Schenter, and A. Morita (2006), Molecular simulations of the transport of molecules across the liquid/vapor interface of water, *Chem. Rev.*, *106*(4), 1355–1374, doi:10.1021/cr040370w.

Gilman, J., and V. Vaida (2006), Permeability of acetic acid through organic films at the air-aqueous interface, *J. Phys. Chem. A*, *110*(24), 7581–7587, doi:10.1021/jp061220n.

Hansson, H. C., M. J. Rood, S. Koloutsou-Vakakis, K. Hameri, D. Orsini, and A. Wiedensohler (1998), Nacl aerosol particle hygroscopicity dependence on mixing with organic compounds, *J. Atmos. Chem.*, *31*(3), 321–346, doi:10.1023/A:1006174514022.

Heikkila, R. E., D. W. Deamer, and D. G. Cornwell (1970), Solution of fatty acids from monolayers spread at air-water interface—Identification of phase transformations and estimation of surface charge, *J. Lipid Res.*, *11*(3), 195–200.

Horn, H. W., W. C. Swope, and J. W. Pitera (2005), Characterization of the TIP4P-Ew water model: Vapor pressure and boiling point, *J. Chem. Phys.*, *123*(19), 194504, doi:10.1063/1.2085031.

Intergovernmental Panel on Climate Change (2007), *Climate Change 2007: The Physical Science Basis: Working Group I Contribution to the Fourth Assessment Report of the IPCC*, edited by S. Solomon et al., Cambridge Univ. Press, New York.

Ishiyama, T., T. Yano, and S. Fujikawa (2004), Molecular dynamics study of kinetic boundary condition at an interface between a polyatomic vapor and its condensed phase, *Phys. Fluids*, *16*(12), 4713–4726, doi:10.1063/1.1811674.

Jakalian, A., B. L. Bush, D. B. Jack, and C. I. Bayly (2000), Fast, efficient generation of high-quality atomic Charges. AM1-BCC model: I. Method, *J. Comput. Chem.*, *21*(2), 132–146, doi:10.1002/(SICI)1096-987X(20000130)21:2<132::AID-JCC5>3.0.CO;2-P.

Kaganer, V. M., H. Mohwald, and P. Dutta (1999), Structure and phase transitions in Langmuir monolayers, *Rev. Mod. Phys.*, *71*(3), 779–819, doi:10.1103/RevModPhys.71.779.

Keene, W. C., A. A. P. Pszenny, J. R. Maben, E. Stevenson, and A. Wall (2004), Closure evaluation of size-resolved aerosol pH in the New England coastal atmosphere during summer, *J. Geophys. Res.*, *109*, D23307, doi:10.1029/2004JD004801.

Kundu, S., and D. Langevin (2008), Fatty acid monolayer dissociation and collapse: Effect of pH and cations, *Colloids Surf. A Physicochem. Eng. Asp.*, *325*(1–2), 81–85, doi:10.1016/j.colsurfa.2008.04.037.

Langevin, D., and C. Griesmar (1980), Light-scattering study of fatty acid monolayers, *J. Phys. D Appl. Phys.*, *13*, 1189–1199, doi:10.1088/0022-3727/13/7/014.

Li, X., T. Hede, Y. Tu, C. Leck, and H. Ågren (2010), Surface-active cis-pinonic acid in atmospheric droplets: A molecular dynamics study, *J. Phys. Chem. Lett.*, *1*(4), 769–773, doi:10.1021/jz9004784.

Li, Y. Q., P. Davidovits, Q. Shi, J. T. Jayne, C. E. Kolb, and D. R. Worsnop (2001), Mass and thermal accommodation coefficients of H_2O(g) on liquid water as a function of temperature, *J. Phys. Chem. A*, *105*(47), 10,627–10,634, doi:10.1021/jp012758q.

Lindahl, E., and O. Edholm (2000), Spatial and energetic-entropic decomposition of surface tension in lipid bilayers from molecular dynamics simulations, *J. Chem. Phys.*, *113*(9), 3882–3893, doi:10.1063/1.1287423.

Liu, L. J. S., R. Burton, W. E. Wilson, and P. Koutrakis (1996), Comparison of aerosol acidity in urban and semirural environments, *Atmos. Environ.*, *30*(8), 1237–1245, doi:10.1016/1352-2310(95)00438-6.

Loader, C. (1999), *Local Regression and Likelihood*, Springer, New York.

Marc, G., and W. McMillan (1985), The virial theorem, *Adv. Chem. Phys.*, *58*, 209–361, doi:10.1002/9780470142820.ch4.

Marek, R., and J. Straub (2001), Analysis of the evaporation coefficient and the condensation coefficient of water, *Int. J. Heat Mass Trans.*, *44*(1), 39–53, doi:10.1016/S0017-9310(00)00086-7.

Martin, S. (2000), Phase transitions of aqueous atmospheric particles, *Chem. Rev.*, *100*(9), 3403–3454, doi:10.1021/cr990034t.

Matsumoto, M. (1998), Molecular dynamics of fluid phase change, *Fluid Phase Equilib.*, *144*(1–2), 307–314, doi:10.1016/S0378-3812(97)00274-4.

Matsumoto, M., and Y. Kataoka (1994), Evaporation and condensation at a liquid surface of methanol, *Mol. Simul.*, *12*(3), 211–217, doi:10.1080/08927029408023031.

Medina, J., and A. Nenes (2004), Effects of film-forming compounds on the growth of giant cloud condensation nuclei: Implications for cloud microphysics and the aerosol indirect effect, *J. Geophys. Res.*, *109*, D20207, doi:10.1029/2004JD004666.

Melzer, V., D. Vollhardt, G. Brezesinski, and H. Mohwald (1998), Similarities in the phase properties of Gibbs and Langmuir monolayers, *J. Phys. Chem. B*, *102*(3), 591–597, doi:10.1021/jp972860g.

Miller, C., and P. Neogi (1985), *Interfacial Phenomena: Equilibrium and Dynamic Effects*, Marcel Dekker, New York.

Mmereki, B., S. Chaudhuri, and D. Donaldson (2003), Enhanced uptake of PAHs by organic-coated aqueous surfaces, *J. Phys. Chem. A*, *107*(13), 2264–2269, doi:10.1021/jp027361g.

Morita, A., and B. C. Garrett (2008), Molecular theory of mass transfer kinetics and dynamics at gas-water interface, *Fluid Dyn. Res.*, *40*(7–8), 459–473, doi:10.1016/j.fluiddyn.2007.12.003.

Morita, A., M. Sugiyama, H. Kameda, S. Koda, and D. R. Hanson (2004), Mass accommodation coefficient of water: Molecular dynamics simulation and revised analysis of droplet train/flow reactor experiment, *J. Phys. Chem. B*, *108*(26), 9111–9120, doi:10.1021/jp030479s.

Nagayama, G., and T. Tsuruta (2003), A general expression for the condensation coefficient based on transition state theory and molecular dynamics simulation, *J. Chem. Phys.*, *118*(3), 1392–1399, doi:10.1063/1.1528192.

Neys, B., and P. Joos (1998), Equilibrium surface tensions and surface potentials of some fatty acids, *Colloids Surf. A*, *143*(2–3), 467–475, doi:10.1016/S0927-7757(98)00610-4.

R Development Core Team (2010), *R: A Language and Environment for Statistical Computing*, 409 pp., R Found. for Stat. Comput., Vienna, Austria.

Ramaswami, A., J. Milford, and M. Small (2005), *Integrated Environmental Modeling: Pollutant Transport, Fate, and Risk in the Environment*, 688 pp., John Wiley, New York.

Raymond, T. M., and S. N. Pandis (2002), Cloud activation of single-component organic aerosol particles, *J. Geophys. Res.*, *107*(D24), 4787, doi:10.1029/2002JD002159.

Roeselová, M., P. Jungwirth, D. Tobias, and R. Gerber (2003), Impact, trapping, and accommodation of hydroxyl radical and ozone at aqueous salt aerosol surfaces. A molecular dynamics study, *J. Phys. Chem. B*, *107*(46), 12,690–12,699, doi:10.1021/jp030592i.

Rogge, W. F., L. M. Hildemann, M. A. Mazurek, G. R. Cass, and B. R. T. Simoneit (1993), Sources of fine organic aerosol. 4. Particulate abrasion products from leaf surfaces of urban plants, *Environ. Sci. Technol.*, *27*(13), 2700–2711, doi:10.1021/es00049a008.

Ruehl, C. R., P. Y. Chuang, and A. Nenes (2008), How quickly do cloud droplets form on atmospheric particles?, *Atmos. Chem. Phys.*, *8*(4), 1043–1055, doi:10.5194/acp-8-1043-2008.

Russell, L. M., S. F. Maria, and S. C. B. Myneni (2002), Mapping organic coatings on atmospheric particles, *Geophys. Res. Lett.*, *29*(16), 1779, doi:10.1029/2002GL014874.

Ryckaert, J., G. Ciccotti, and H. Berendsen (1977), Numerical integration of the Cartesian equations of motion of a system with constraints: Molecular dynamics of n-alkanes, *J. Comput. Phys.*, *23*(3), 327–341, doi:10.1016/0021-9991(77)90098-5.

Schauer, J. J., M. J. Kleeman, G. R. Cass, and B. R. T. Simoneit (1999), Measurement of emissions from air pollution sources. 1. C-1 through C-29 organic compounds from meat charbroiling, *Environ. Sci. Technol.*, *33*(10), 1566–1577, doi:10.1021/es980076j.

Seidl, W. (2000), Model for a surface film of fatty acids on rainwater and aerosol particles, *Atmos. Environ.*, *34*(28), 4917–4932, doi:10.1016/S1352-2310(00)00198-9.

Seinfeld, J., and S. Pandis (2006), *Atmospheric Chemistry and Physics: From Air Pollution to Climate Change*, 1232 pp., John Wiley, New York.

Shantz, N., R. Chang, J. Slowik, A. Vlasenko, J. Abbatt, and W. Leaitch (2010), Slower CCN growth kinetics of anthropogenic aerosol compared to biogenic aerosol observed at a rural site, *Atmos. Chem. Phys.*, *10*, 299–312, doi:10.5194/acp-10-299-2010.

Siu, S. W. I., R. Vacha, P. Jungwirth, and R. A. Bockmann (2008), Biomolecular simulations of membranes: Physical properties from different force fields, *J. Chem. Phys.*, *128*(12), 125103, doi:10.1063/1.2897760.

Smith, W., C. Yong, and P. Rodger (2002), DL_POLY: Application to molecular simulation, *Mol. Simul.*, *28*(5), 385–471, doi:10.1080/08927020290018769.

Sorjamaa, R., B. Svenningsson, T. Raatikainen, S. Henning, M. Bilde, and A. Laaksonen (2004), The role of surfactants in Köhler theory reconsidered, *Atmos. Chem. Phys.*, *4*, 2107–2117, doi:10.5194/acp-4-2107-2004.

Takahama, S., S. Liu, and L. M. Russell (2010), Coatings and clusters of carboxylic acids in carbon-containing atmospheric particles from spectromicroscopy and their implications for cloud-nucleating and optical properties, *J. Geophys. Res.*, *115*, D01202, doi:10.1029/2009JD012622.

Taylor, R., D. Ray, and B. Garrett (1997), Understanding the mechanism for the mass accommodation of ethanol by a water droplet, *J. Phys. Chem. B*, *101*(28), 5473–5476, doi:10.1021/jp9706442.

Tervahattu, H., and J. Juhanoja (2002), Identification of an organic coating on marine aerosol particles by tof-sims, *J. Geophys. Res.*, *107*(D16), 4319, doi:10.1029/2001JD001403.

Tervahattu, H., J. Juhanoja, V. Vaida, A. F. Tuck, J. V. Niemi, K. Kupiainen, M. Kulmala, and H. Vehkamaki (2005), Fatty acids on continental sulfate aerosol particles, *J. Geophys. Res.*, *110*, D06207, doi:10.1029/2004JD005400.

Tieleman, D. P., S. J. Marrink, and H. J. C. Berendsen (1997), A computer perspective of membranes: Molecular dynamics studies of lipid bilayer systems, *Biochim. Biophys. Acta*, *1331*(3), 235–270.

Torn, R., and G. Nathanson (2002), Surface tensions and surface segregation of n-butanol in sulfuric acid, *J. Phys. Chem. B*, *106*(33), 8064–8069, doi:10.1021/jp020253+.

Tsuruta, T., and G. Nagayama (2004), Molecular dynamics studies on the condensation coefficient of water, *J. Phys. Chem. B*, *108*(5), 1736–1743, doi:10.1021/jp035885q.

Vega, C., and E. de Miguel (2007), Surface tension of the most popular models of water by using the test area simulation method, *J. Chem. Phys.*, *126*(15), 154707, doi:10.1063/1.2715577.

Vieceli, J., M. Roeselová, and D. J. Tobias (2004), Accommodation coefficients for water vapor at the air/water interface, *Chem. Phys. Lett.*, *393*(1–3), 249–255, doi:10.1016/j.cplett.2004.06.038.

Vieceli, J., M. Roeselová, N. Potter, L. X. Dang, B. C. Garrett, and D. J. Tobias (2005), Molecular dynamics simulations of atmospheric oxidants at the air-water interface: Solvation and accommodation of OH and O_3, *J. Phys. Chem. B*, *109*(33), 15,876–15,892, doi:10.1021/jp051361+.

Wang, J. M., R. M. Wolf, J. W. Caldwell, P. A. Kollman, and D. A. Case (2004), Development and testing of a general amber force field, *J. Comput. Chem.*, *25*(9), 1157–1174, doi:10.1002/jcc.20035.

Wang, J. M., W. Wang, P. A. Kollman, and D. A. Case (2006), Automatic atom type and bond type perception in molecular mechanical calculations, *J. Mol. Graph. Model.*, *25*(2), 247–260, doi:10.1016/j.jmgm.2005.12.005.

Wilson, M. A., and A. Pohorille (1997), Adsorption and solvation of ethanol at the water liquid-vapor interface: A molecular dynamics study, *J. Phys. Chem. B*, *101*(16), 3130–3135, doi:10.1021/jp962629n.

Zhang, Q., J. L. Jimenez, D. R. Worsnop, and M. Canagaratna (2007), A case study of urban particle acidity and its influence on secondary organic aerosol, *Environ. Sci. Technol.*, *41*, 3213–3219, doi:10.1021/es061812j.

L. M. Russell and S. Takahama, Scripps Institution of Oceanography, University of California, San Diego, 9500 Gilman Dr., Mail Code 0221, La Jolla, CA 92093-0221, USA. (lmrussell@ucsd.edu)